Atomic-layered Au clusters on α-MoC as catalysts for the low-temperature water-gas shift reaction

Siyu Yao,[1]* Xiao Zhang,[2]* Wu Zhou,[3,4]* Rui Gao,[5,6] Wenqian Xu,[7] Yifan Ye,[8] Lili Lin,[1] Xiaodong Wen,[5,6] Ping Liu,[7] Bingbing Chen,[2] Ethan Crumlin,[8] Jinghua Guo,[8] Zhijun Zuo,[9] Weizhen Li,[1] Jinglin Xie, [1] Li Lu,[10] Christopher J. Kiely,[10] Lin Gu,[11] Chuan Shi,[2]† José A. Rodriguez,[7]† Ding Ma[1]†

[1]College of Chemistry and Molecular Engineering and College of Engineering, Peking University, Beijing 100871, China. [2]State Key Laboratory of Fine Chemicals, College of Chemistry, Dalian University of Technology, Dalian 116024, China. [3]School of Physical Sciences, CAS Key Laboratory of Vacuum Sciences, University of Chinese Academy of Sciences, Beijing 100049, China. [4]Materials Science and Technology Division, Oak Ridge National Laboratory, Oak Ridge, TN 37831, USA. [5]State Key Laboratory of Coal Conversion, Institute of Coal Chemistry, Chinese Academy of Sciences, Post Office Box 165, Taiyuan, Shanxi 030001, China. [6]Synfuels China, Beijing, 100195, China.
[7]Chemistry Department, Building 555, Brookhaven National Laboratory, Post Office Box 5000, Upton, NY 11973-5000, USA. [8]Advanced Light Source, Lawrence Berkeley National Laboratory, Berkeley, CA 94720, USA. [9]Key Laboratory of Coal Science and Technology of Ministry of Education and Shanxi Province, Taiyuan University of Technology, Taiyuan 030024, Shanxi, China. [10]Department of Materials Science and Engineering, Lehigh University, Bethlehem, PA 18015-3195, USA. [11]Institute of Physics, Chinese Academy of Sciences, Beijing 100190, China.
*These authors contributed equally to this work.

†Corresponding author. Email: chuanshi@dlut.edu.cn (C.S.); rodrigez@bnl.gov (J.A.R.); dma@pku.edu.cn (D.M.)

The water-gas shift (WGS) reaction ($CO+H_2O=H_2+CO_2$) is an essential process for hydrogen generation and CO removal in various energy-related chemical operations. This equilibrium-limited reaction is favored at a low working temperature. Potential application in fuel cells also requires a WGS catalyst to be highly active, stable and energy-efficient and match the working temperature of on-site hydrogen generation and consumption units. We synthesized Au layered clusters on an α-MoC substrate to create an interfacial catalyst system for the ultra-low-temperature WGS reaction. Water was activated over α-MoC at 303 Kelvin (K), while CO adsorbed on adjacent Au sites is apt to react with surface hydroxyl groups formed from water splitting, leading to a high WGS activity at low-temperatures.

Low-temperature efficient catalysts for the WGS reaction, especially those operating under 423 K (*1–7*), are of interest for applications in fuel cells, especially those use H_2 generated by hydrocarbon reforming processes that are contaminated with CO, which deactivates the catalysts. For the heterogeneous catalysis, besides Cu based catalysts which display low activity at low temperature, (*8, 9*) Pt group noble metals and Au supported on reducible metal oxides, like ceria (*1*) or FeO_x (*10*) which contain oxygen-vacancies, are commonly used. Flytzani-Stephanopoulos and co-workers demonstrated that noble metal catalysts dispersed on alkali promoted inert supports can also be active for WGS, making a reducible oxide support no longer a requirement (*4*, *6*). The alkali ion-associated surface -OH groups are reactive toward CO in the presence of atomically dispersed platinum or gold, giving the catalyst superior metal atom efficiency in the WGS reaction. Metal carbide, (*e.g.* hexagonal closest packing (hcp) β-Mo_2C) supported noble metal catalysts provide similar functionalities and are more active for the reaction at low temperature (*7*, *11*, *12*). However, none of these systems displays an activity higher than 0.1 $mol_{CO}/(mol_{metal}\cdot s)$ between 393 and 423 K (Table 1).

In order to achieve high WGS activity at low tempera-ture, we searched for catalysts that could dissociate water efficiently and reform the generated oxygen-containing spe-cies (reaction of surface oxygen or hydroxyl with CO*) at low temperature. We report that Au confined over face cen-tered cubic (fcc) structured α-MoC is at least one order of magnitude more active than previous reports for the WGS reaction below 423 K. The α-MoC substrate facilitates epi-taxially-grown atomic Au layers with altered electronic structure for favorable bonding with CO. Its synergy with adjacent Mo sites in α-MoC can effectively activate water at low temperature.

Gold supported over pure phase α-MoC catalysts were synthesized by a precipitation method followed by sequen-tial temperature programmed ammonization and carburiza-tion. For comparative purposes, α-MoC, 2wt%Au/β-Mo_2C (*13*, *14*), 2wt%Au/SiO_2 (*15*) and 2wt%Au/CeO_2 (*1*) catalysts were also prepared. The high dispersion of Au for the 2wt%Au/α-MoC catalyst was evidenced by the lack of x-ray diffraction (XRD) peaks associated with Au crystallites. Operando XRD studies (1% CO-3% H_2O-He, 10 ml/min) revealed that the bulk structure of the 2%Au/α-MoC catalyst remained intact up to 523 K, beyond which the α-MoC was gradually oxi-dized by water (Fig. 1A). Ex-situ XRD experiments (10.5%CO-21%H_2O-20%N_2-Ar, GHSV=180,000/h) confirmed that at higher water partial pressure, the bulk structure of

catalysts is stable up to 473 K. Neither the oxidation of α-MoC nor the aggregation of Au was observed at tempera-tures up to 473 K (fig. S1).

The WGS activity was evaluated under product-free (10.5%CO-21%H_2O-20%N_2-Ar) and full reformate gas feeds (11%CO-26%H_2O-26%H_2-7%CO_2-N_2). In the product-free gas (GSVH=180,000 hours^{-1}), α-MoC shows very low CO conver-sion (3.4%) at 393 K (Fig. 1B), and none of the reference cat-alysts achieved > 5% CO conversion < 423 K. However, for the 2%Au/α-MoC catalyst, CO conversion was > 95% at 393 K and reaching 98% at only 423 K. For reaction tempera-tures to 523 K and beyond, CO conversion dropped, which may result from the thermodynamic limitation as well as the gradual transformation of α-MoC to molybdenum oxide, as confirmed by the operando XRD results (Fig. 1A and fig. S2). The Au normalized activity of the 2%Au/α-MoC catalyst in product-free gas was 0.012, 0.13, 1.05, 1.66 and 3.19 $mol_{CO}/(mol_{Au}*s)$ at 313, 353, 393, 423 and 473 K, respectively, this high activity at low temperatures compares favorably with other reported WGS catalysts (Table 1, fig. S3, CO con-version below 15%). Due to the limitation of the water satu-ration vapor pressure, at low temperature the composition of reactant gas was adjusted). We determined that 2% is the optimal Au loading for the Au/α-MoC catalyst (fig. S4).

In full reformate gas feed under similar space velocity, the activity dropped slightly (62% activity at 393 K) because of product (H_2 and CO_2) inhibition (Fig. 1D). However, the activity of the 2%Au/α-MoC catalyst remained as high as 0.62 s^{-1} and 2.02 s^{-1} at 393 and 473 K, respectively. The ap-parent barriers E_{app} of α-MoC itself is actually low E_{app} value of 58 ± 10 kJ/mol, and even lower for the 2%Au/α-MoC cata-lyst, 22 ± 1 kJ/mol. Thus, the addition of Au greatly en-hanced the low-temperature reactivity of a good WGS catalyst (Fig. 1E). Its exceptional activity and high equilibri-um CO conversion at low temperature can be exploited sim-ultaneously (fig. S5), and the catalyst shows an excellent total turnover number (TTN), reaching up to 385400 mol_{CO}/mol_{Au} in a single-run reaction (fig. S6 and table S1).

We designed a two-step temperature programmed sur-face reaction (TPSR) experiment to explore the reaction route. After pre-activation of the catalysts, 2% H_2O/Ar (100 ml/min, 10 min) was introduced into the reactor at 303 K. Production of H_2 was immediately observed on both 2%Au/α-MoC and α-MoC catalysts, indicating the presence of a low-temperature water dissociation center on α-MoC that led to the formation of H_2 and surface OH species (Fig. 2, A and B; see also figs. S7 and S8). In contrast, no H_2 pro-duction was observed on 2%Au/SiO_2 or 2%Au/β-Mo_2C cata-lysts (Fig. 2C and fig. S9). After purging with Ar (100 ml/min), the system was then switched to 2% CO/Ar (100 ml/min) at 303 K, and kept at that temperature for 10 min and then increased to 523 K at 5 K/min. For the Au/SiO_2 catalyst, only water desorption was observed at ~ 403 K. In sharp contrast, CO_2 and H_2 were detected simultaneously on the 2%Au/α-MoC catalyst at around 308 K and their intensi-ties reached the maxima at 367 K. Thus, the reaction of CO with surface OH could occur at very low temperature (308 K) to form CO_2 and additional H_2. The reforming reaction can also happen on α-MoC catalyst, but initiating at a much higher initialing temperature (347 K).

The co-existence of a low-temperature water dissociation center on α-MoC and the low-temperature reforming center over the 2% Au/α-MoC catalyst is the key for the extraordi-nary activity of this catalyst. The Au L_3 edge extended x-ray absorption fine structure (EXAFS) fitting (table S2 and fig. S10) shows a low Au-Au first shell coordination number(CN) of 6.9 indicates that the average size of Au species is ~ 1.5 nm for a hemispherical morphology (*16*). The Au-Mo CN of 1.6 is particularly striking given that Au nanoparticles (NPs) tend to undergo sintering because of the low Tammann temperature (668 K) of bulk Au. (*17*, *18*) Given that this sample was activated at 973 K for more than 2 hours, a strong metal-support interaction must exist between Au and α-MoC. X-ray photoelectron spectroscopy (XPS) (fig. S11) revealed that the Au 4*f* binding energy shifted 0.6 eV to higher energy with respect to bulk gold (*19*), indicating that the electronic structure of the Au species is perturbed by the substrate. The reaction order of CO of -0.16 (Fig. 1D), also indicated that CO was already relatively strongly adsorbed on the electronically modified Au surface.

Aberration-corrected scanning transmission electron mi-croscopy (STEM) analysis on the 2%Au/α-MoC catalyst showed that the catalyst supports were porous assemblies of small α-MoC NPs (3 to 20 nm in diameter, fig. S12). High resolution STEM Z-contrast imaging (Fig. 2, D and E) re-vealed two types of Au species on the surface of α-MoC, small Au layered clusters epitaxially grown on the α-MoC support and atomically dispersed Au. The epitaxial Au clus-ters had an average diameter of 1 to2 nm and thickness of 2 to 4 atomic layers (<1 nm), as measured from edge-on clus-ters occasionally found in profile view (Fig. 2E and fig. S13). Detailed crystal structure analysis (fig. S12, C and D) also showed that these epitaxial Au clusters strongly aligned with the (111) planes of the α-MoC support, with some ex-posed (200) facets. There were no larger Au NPs present in this sample (fig. S14). No obvious structural difference was observed between the fresh and the used catalyst samples (Fig. 2F), and both types of Au species were retained in the tested sample, which is also consistent with the relatively good stability of the catalyst noted in the catalytic reaction.

We used NaCN solution to selectively leach the layered Au clusters from the 2% Au/α-MoC catalyst (*1*, *20*). The Au loading decreased to around 0.9 wt%, leaving predominant-ly the atomically dispersed Au atoms, which was confirmed

by both STEM and XAFS results (Fig. 2G; fig. S12, E to G; and table S2). The Au normalized WGS activity of 0.9% Au/α-MoC (NaCN) at 393 and 423 K decreased to around 1/11 and 1/6 of their original values respectively, but was still higher than that of NaCN-leached α-MoC catalyst (with acti-vation barrier similar to that of fresh α-MoC, Fig. 1E). This result indicated that atomically dispersed Au species were indeed catalytically active (*1*), but the catalytic efficacy of the layered Au clusters on α-MoC support for low tempera-ture WGS was even higher than the atomically dispersed Au. Furthermore, the E_{app} increased to 41 kJ/mol after NaCN leaching (Fig. 1E), suggesting some degree blocking of the low-temperature reaction route after the removal of layered Au clusters. Thus, we attribute the low-temperature WGS activity mainly to the epitaxial Au clusters decorating the α-MoC support.

We carried out DFT calculations to investigate the WGS reaction path on the Au/α-MoC catalyst. Three catalyst models (see fig. S15) of Au (111), monolayer Au/α-MoC (111) and cluster Au_{15}/α-MoC (111) were constructed to represent the different sites on Au/α-MoC, in which Au (111) and mon-olayer Au/α-MoC (111) simulate large Au NPs and electronic property modified Au NPs, respectively. Au_{15}/α-MoC (111) represents the interface model of our atomic-layered Au cluster over α-MoC (111). Similar to experimental observa-tions, the Au cluster in Au_{15}/α-MoC has a layered structure, with (111) and (200) type exposed facets.

As shown in fig. S16, H_2O is hard to dissociate on Au (111)and monolayer Au/α-MoC (111) thermodynamically and kinetically, with barriers of 1.91 and 1.66 eV, and the reac-tions are endothermic by 1.57 and 1.15 eV, respectively. In contrast, when we investigated the first step of WGS, name-ly water dissociation, on Au_{15}/α-MoC (111), we found that at lower coverage (Fig. 3A), two H_2O molecules could be easily dissociated and form two H atoms and two OH species with the effective barrier of 0.77 eV ($CO + 2H_2O \rightarrow CO + 2OH + 2H$), and the two OH can immediately react (and without barrier), forming a surface O atom ($CO + 2OH + 2H \rightarrow CO + H_2O + O + 2H$, it is exothermic by 0.38 eV). These results indicate that some surface domains of α-MoC could be oxi-dized by water during the reaction, which has been con-firmed by XPS and ^{18}O nuclear magnetic resonance experiments (figs. S7 and S8). After the surface was partially decorated with oxygen (Fig. 3B), the calculations found that surface O atoms could further promote water dissociation.

The successive O-assisted water dissociation ($CO + 3O + H_2O \rightarrow CO + 2O + 2OH$) on the boundary of Au_{15} and α-MoC (111) had a much lower barrier of 0.22 eV, indicating that the first O-H bond of water could be easily broken at low temperature by this bifunctional catalyst.

The formed surface OH species on the Mo site was apt to react with CO adsorbed on the adjacent Au surface, which has the right geometry (triangular) to enable a low reaction barrier. Indeed, at low CO coverage (Fig. 3A), the effective barrier for the reforming of CO on Au and OH on α-MoC (111)is 0.72 eV, including a migration barrier of 0.22 eV and the reaction barrier of 0.50 eV. At high CO coverage (Fig. 3C), the reforming barrier was even lower, *i.e.* 0.52 eV, demonstrating that the reaction between adsorbed CO and surface OH species on the peripheral interface of Au and α-MoC ($CO+OH=CO_2+ \frac{1}{2}H_2$) was apt to proceed. Although the reforming process was facile, it still had a higher barrier than the first step of the WGS reaction, i.e., water dissocia-tion on partially oxidized α-MoC. Thus, the rate-determining step of the WGS process over Au_{15}/α-MoC is the reforming process, which is in good agreement with our TPSR observa-tions (Fig. 2). The interfacial nature and optimum bonding of this α-MoC confined Au nanostructure that confers the catalyst with outstanding WGS reactivity at low tempera-ture.

REFERENCES AND NOTES

1. Q. Fu, H. Saltsburg, M. Flytzani-Stephanopoulos, Active nonmetallic Au and Pt species on ceria-based water-gas shift catalysts. *Science* **301**, 935–938 (2003). doi:10.1126/science.1085721 Medline
2. J. A. Rodriguez, S. Ma, P. Liu, J. Hrbek, J. Evans, M. Pérez, Activity of CeOx and TiOx nanoparticles grown on Au(111) in the water-gas shift reaction. *Science* **318**, 1757–1760 (2007). doi:10.1126/science.1150038 Medline
3. J. A. Rodriguez, J. Graciani, J. Evans, J. B. Park, F. Yang, D. Stacchiola, S. D. Senanayake, S. Ma, M. Pérez, P. Liu, J. Fdez Sanz, J. Hrbek, Water-gas shift reaction on a highly active inverse CeO_x/Cu(111) catalyst: Unique role of ceria nanoparticles. *Angew. Chem. Int. Ed.* **48**, 8047–8050 (2009). doi:10.1002/anie.200903918 Medline
4. Y. Zhai, D. Pierre, R. Si, W. Deng, P. Ferrin, A. U. Nilekar, G. Peng, J. A. Herron, D. C. Bell, H. Saltsburg, M. Mavrikakis, M. Flytzani-Stephanopoulos, Alkali-stabilized Pt-OH_x species catalyze low-temperature water-gas shift reactions. *Science* **329**, 1633–1636 (2010). doi:10.1126/science.1192449 Medline
5. M. Yang, S. Li, Y. Wang, J. A. Herron, Y. Xu, L. F. Allard, S. Lee, J. Huang, M. Mavrikakis, M. Flytzani-Stephanopoulos, Catalytically active Au-$O(OH)_x$-species stabilized by alkali ions on zeolites and mesoporous oxides. *Science* **346**, 1498– 1501 (2014). doi:10.1126/science.1260526 Medline
6. M. Yang, L. F. Allard, M. Flytzani-Stephanopoulos, Atomically dispersed Au-$(OH)_x$ species bound on titania catalyze the low-temperature water-gas shift reaction. *J. Am. Chem. Soc.* **135**, 3768–3771 (2013). doi:10.1021/ja312646d *Medline*
7. J. A. Rodriguez, P. J. Ramírez, G. G. Asara, F. Viñes, J. Evans, P. Liu, J. M. Ricart, F. Illas, Charge polarization at a Au-TiC interface and the generation of highly active and selective catalysts for the low-temperature water-gas shift reaction. *Angew. Chem. Int. Ed.* **53**, 11270–11274 (2014). doi:10.1002/anie.201407208 *Medline*
8. Y. Li, Q. Fu, M. Flytzani-Stephanopoulos, Low-temperature water-gas shift reaction over Cu- and Ni-loaded cerium oxide catalysts. *Appl. Catal. B* **27**, 179– 191 (2000). doi:10.1016/S0926-3373(00)00147-8
9. C. Ratnasamy, J. P. Wagner, Water gas shift catalysis. *Catal. Rev.* **51**, 325–440 (2009). doi:10.1080/01614940903048661
10. D. Andreeva, V. Idakiev, T. Tabakova, A. Andreev, Low-temperature water–gas shift reaction over Au/α-Fe2O3. *J. Catal.* **158**, 354–355 (1996). doi:10.1006/jcat.1996.0035
11. N. M. Schweitzer, J. A. Schaidle, O. K. Ezekoye, X. Pan, S. Linic, L. T. Thompson, High activity carbide supported catalysts for water gas shift. *J. Am. Chem. Soc.* **133**, 2378–2381 (2011). doi:10.1021/ja110705a **Medline**
12. K. D. Sabnis, Y. Cui, M. C. Akatay, M. Shekhar, W.-S. Lee, J. T. Miller, W. N. Delgass, F. H. Ribeiro, Water–gas shift catalysis over transition metals supported on molybdenum carbide. *J. Catal.* **331**, 162–171 (2015). doi:10.1016/j.jcat.2015.08.017

13. J. S. Lee, S. T. Oyama, M. Boudart, Molybdenum carbide catalysts: I. Synthesis of unsupported powders. *J. Catal.* **106**, 125–133 (1987). doi:10.1016/0021-9517(87)90218-1
14. S. T. Oyama, Preparation and catalytic properties of transition metal carbides and nitrides. *Catal. Today* **15**, 179–200 (1992). doi:10.1016/0920-5861(92)80175-M
15. K. Qian, L. Luo, H. Bao, Q. Hua, Z. Jiang, W. Huang, Catalytically active structures of SiO_2-supported Au nanoparticles in low-temperature CO oxidation. *Catal. Sci. Technol.* **3**, 679–687 (2013). doi:10.1039/C2CY20481A
16. A. M. Beale, B. M. Weckhuysen, EXAFS as a tool to interrogate the size and shape of mono and bimetallic catalyst nanoparticles. *Phys. Chem. Chem. Phys.* **12**, 5562–5574 (2010). doi:10.1039/b925206a Medline
17. M. Haruta, Gold catalysts prepared by coprecipitation for low-temperature oxidation of hydrogen and of carbon monoxide. *J. Catal.* **115**, 301–309 (1989). doi:10.1016/0021-9517(89)90034-1
18. G. M. Veith, A. R. Lupini, S. Rashkeev, S. J. Pennycook, D. R. Mullins, V. Schwartz, C. A. Bridges, N. J. Dudney, Thermal stability and catalytic activity of gold nanoparticles supported on silica. *J. Catal.* **262**, 92–101 (2009). doi:10.1016/j.jcat.2008.12.005
19. R. Si, M. Flytzani-Stephanopoulos, Shape and crystal-plane effects of nanoscale ceria on the activity of Au-CeO_2 catalysts for the water-gas shift reaction. *Angew. Chem. Int. Ed.* **47**, 2884–2887 (2008). doi:10.1002/anie.200705828 *Medline*
20. N. Hedley, H. Tabachnik, *Chemistry of Cyanadation* (American Cyanamid Company, 1968).
21. J. Lin, A. Wang, B. Qiao, X. Liu, X. Yang, X. Wang, J. Liang, J. Li, J. Liu, T. Zhang, Remarkable performance of Ir_1/FeO_x single-atom catalyst in water gas shift reaction. *J. Am. Chem. Soc.* **135**, 15314–15317 (2013). doi:10.1021/ja408574m Medline
22. W. Deng, C. Carpenter, N. Yi, M. Flytzani-Stephanopoulos, Comparison of the activity of Au/CeO_2 and Au/Fe_2O_3 catalysts for the CO oxidation and the water-gas shift reactions. *Top. Catal.* **44**, 199–208 (2007). doi:10.1007/s11244-007-0293-9
23. B. Zugic, S. Zhang, D. C. Bell, F. F. Tao, M. Flytzani-Stephanopoulos, Probing the low-temperature water-gas shift activity of alkali-promoted platinum catalysts stabilized on carbon supports. *J. Am. Chem. Soc.* **136**, 3238–3245 (2014). doi:10.1021/ja4123889 Medline
24. R. M. Laine, R. G. Rinker, P. C. Ford, Homogeneous catalysis by ruthenium carbonyl in alkaline solution: The water gas shift reaction. *J. Am. Chem. Soc.* **99**, 252–253 (1977). doi:10.1021/ja00443a049
25. A. Hammersley, *European Synchrotron Radiation Facility Internal Report ESRF97HA02T 68* (European Synchrotron Radiation Facility, 1997).
26. B. Ravel, M. Newville, *ATHENA*, *ARTEMIS*, *HEPHAESTUS*: Data analysis for X-ray absorption spectroscopy using *IFEFFIT*. *J. Synchrotron Radiat.* **12**, 537–541 (2005). doi:10.1107/S0909049505012719 Medline
27. D. Mendes, A. Mendes, L. M. Madeira, A. Iulianelli, J. M. Sousa, A. Basile, The water-gas shift reaction: From conventional catalytic systems to Pd-based membrane reactors-a review. *Asia-Pac. J. Chem. Eng.* **5**, 111–137 (2010). doi:10.1002/apj.364
28. G. Kresse, J. Furthmuller, Efficiency of ab-initio total energy calculations for metals and semiconductors using a plane-wave basis set. *Comput. Mater. Sci.* **6**, 15–50 (1996). doi:10.1016/0927-0256(96)00008-0
29. G. Kresse, J. Furthmüller, Efficient iterative schemes for *ab initio* total-energy calculations using a plane-wave basis set. *Phys. Rev. B* **54**, 11169–11186 (1996). doi:10.1103/PhysRevB.54.11169 Medline
30. P. E. Blöchl, Projector augmented-wave method. *Phys. Rev. B* **50**, 17953–17979 (1994). doi:10.1103/PhysRevB.50.17953 Medline
31. G. Kresse, D. Joubert, From ultrasoft pseudopotentials to the projector augmented-wave method. *Phys. Rev. B* **59**, 1758–1775 (1999). doi:10.1103/PhysRevB.59.1758
32. J. P. Perdew, K. Burke, M. Ernzerhof, Generalized gradient approximation made simple. *Phys. Rev. Lett.* **77**, 3865–3868 (1996). doi:10.1103/PhysRevLett.77.3865 Medline
33. G. Henkelman, B. P. Uberuaga, H. Jonsson, A climbing image nudged elastic band method for finding saddle points and minimum energy paths. *J. Chem. Phys.* **113**, 9901–9904 (2000). doi:10.1063/1.1329672
34. Q. Li, R. He, J. O. Jensen, N. J. Bjerrum, PBI-based polymer membranes for high temperature fuel cells – preparation, characterization and fuel cell demonstration. *Fuel Cells (Weinh.)* **4**, 147–159 (2004). doi:10.1002/fuce.200400020
35. M. D. Porosoff, X. Yang, J. A. Boscoboinik, J. G. Chen, Molybdenum carbide as alternative catalysts to precious metals for highly selective reduction of CO_2 to CO. *Angew. Chem. Int. Ed.* **53**, 6705–6709 (2014). doi:10.1002/anie.201404109 Medline
36. P. Zhang, T. K. Sham, Tuning the electronic behavior of Au nanoparticles with capping molecules. *Appl. Phys. Lett.* **81**, 736–738 (2002). doi:10.1063/1.1494120
37. Q. Fu, W. Deng, H. Saltsburg, M. Flytzani-Stephanopoulos, Activity and stability of low-content gold–cerium oxide catalysts for the water–gas shift reaction. *Appl. Catal. B* **56**, 57–68 (2005). doi:10.1016/j.apcatb.2004.07.015
38. N. Ta, J. J. Liu, S. Chenna, P. A. Crozier, Y. Li, A. Chen, W. Shen, Stabilized gold nanoparticles on ceria nanorods by strong interfacial anchoring. *J. Am. Chem. Soc.* **134**, 20585–20588 (2012). doi:10.1021/ja310341j *Medline*

ACKNOWLEDGMENTS

This work received financial support from 973 Project (2017YFB0602200, 2013CB933100, 2011CB201402), CAS Pioneer Hundred Talents Program, and the Natural Science Foundation of China (91645115, 21473003, 21222306, 21373037, 21577013 and 91545121). The electron microscopy work was also supported in part by the U.S. Department of Energy, Office of Science, Basic Energy Science, Materials Sciences and Engineering Division (W.Z.), and through a user project at ORNL's Center for Nanophase Materials Sciences (CNMS), which is a DOE Office of Science User Facility. The XAS experiments were conducted in SSRF and BSRF. We also acknowledge National Thousand Young Talents Program of China, the CAS Hundred Talents Program, the Shanxi Hundred Talent Program and the Fundamental Research Funds for the Central Universities (No. DUT15TD49 and DUT16ZD224). The research done at Brookhaven National Laboratory (BNL) was financed under Contract No.DE-SC0012704 with the U.S. Department of Energy. Part of the theoretical calculations were done at the Center for Functional Nanomaterials in the BNL campus. The Advanced Light Source is supported by the Director, Office of Science, Office of Basic Energy Sciences, of the U.S. Department of Energy under Contract No. DE-AC02-05CH11231. YY acknowledges the support of the ALS Doctorial Fellowship. CJK gratefully acknowledges funding from the National Science Foundation Major Research Instrumentation program (GR# MRI/DMR-1040229). D.M thanks L. Peng and M. Wang for help in ^{17}O NMR experiments. All data are reported in the man text and supplement. C. S. and X.Z. are inventors on patent application (ZL 2015 1 0253637.6) held by Dalian University of Technology that covers the preparation of Au/α-MoC. Author contributions: D.M, C.S., and J. A. R., designed the study. X. Z. and S. Y. performed most of the reactions. W. Z., L.L., C.J.K., and L.G. performed the electron microscopy study. R.G, X.-D.W., P. L., and Z. Z. finished the DFT calculation. S.Y., Q.W. and W.L. performed the X-ray structure characterization and analysis. S.Y., D.M., W.Z., and J.A.R. wrote the paper. Other authors provided reagents, performed the certain experiments and revised the paper.

Table 1. Comparison of the activities over the representative catalytic systems for low-temperature WGS reaction.

	Temp (K)	Gas feed composition	Mass specific activity [$\mu mol_{CO}/(g_{cat} \cdot s)$]	Metal normalized activity [$mol_{CO}/(mol_{metal} \cdot s)$]	Apparent activation energy (kJ/mol)	Ref
Reducible oxide supports						
Au/CeO_2	523	11%CO-26%H_2O-26%H_2-7%CO_2-He	4.8	0.13	37	(*1*)
Pt/CeO_2	523	11%CO-26%H_2O-26%H_2-7%CO_2-He	22	0.17	75	(*1*)
Ir_1/FeO_x	573	2%CO-10%H_2O-He	1.2	2.32	50	(*21*)
Au/FeO_x	598	11%CO-26%H_2O-26%H_2-7%CO_2-He	11	0.31	49	(*22*)
Alkali promoted inert supports						
Au-Na/MCM41	423	11%CO-26%H_2O-26%H_2-7%CO_2-He	0.8	0.067	44	(*5*)
Pt-Na/SiO_2	523	11%CO-26%H_2O-26%H_2-7%CO_2-He	12	0.24	70	(*4*)
Pt-Na/CNT	473	2%CO-10%H_2O-He	1.25	0.024	70	(*23*)
Molybdenum carbide supports (β-Mo_2C)						
Pt/Mo_2C	513	11%CO-21%H_2O-43%H_2-6%CO_2-N_2	221	1.42	53	(*11*)
Pt/Mo_2C	393	7%CO-22%H_2O-37%H_2-8.5%CO_2-Ar	1.8	0.023	48	(*12*)
Au/Mo_2C	393	7%CO-22%H_2O-37%H_2-8.5%CO_2-Ar	1.6	0.021	44	(*12*)
Homogeneous catalysts						
$Ru_3(CO)_{12}$	373	1 bar CO/NaOH solution	0.12	2.6 E-5	-	(*24*)
Our results						
2% Au/α-MoC	313	3%CO-6%H_2O-20%N_2-Ar	1.22	0.012		-
	333	5%CO-10%H_2O-20%N_2-Ar	5.91	0.06		
	353		13.06	0.13		
	393	10.5%CO-21%H_2O-20%N_2-Ar	103	1.05	22†	
	423		167	1.66		
	473		325	3.19		
2% Au/α-MoC	333	5%CO-10%H_2O-10%H_2-3%CO_2-N_2	2.39	0.02		-
	353		9.20	0.09		
	393	11%CO-26%H_2O-26%H_2-7%CO_2-N_2	53	0.62	27	
	423		106	1.05		
	473		213	2.02		
0.9% Au/α-MoC (NaCN)	393	10.5%CO-21%H_2O-20%N_2-Ar	9.07	0.09	41	-
	423		26.6	0.26		
	473		73.1	0.72		
2%Au/β-Mo_2C	393	11%CO-26%H_2O-26%H_2-7%CO_2-N_2	2.06	0.02	38	-
	423		4.29	0.04		
	473		14.4	0.14		
α-MoC	393	11%CO-26%H_2O-26%H_2-7%CO_2-N_2	2.05		64	-
	423		8.57			
	473		56.7			
2% Au/SiO_2	673	10.5%CO-21%H_2O-20%N_2-Ar	0.24	2.4 E-3		
2% Au/CeO_2	423	11%CO-26%H_2O-26%H_2-7%CO_2-N_2	1.1	0.01		

*The operating pressure of the catalysts listed is 1 bar. †The activation energy was also determined by another method, see fig. S17.

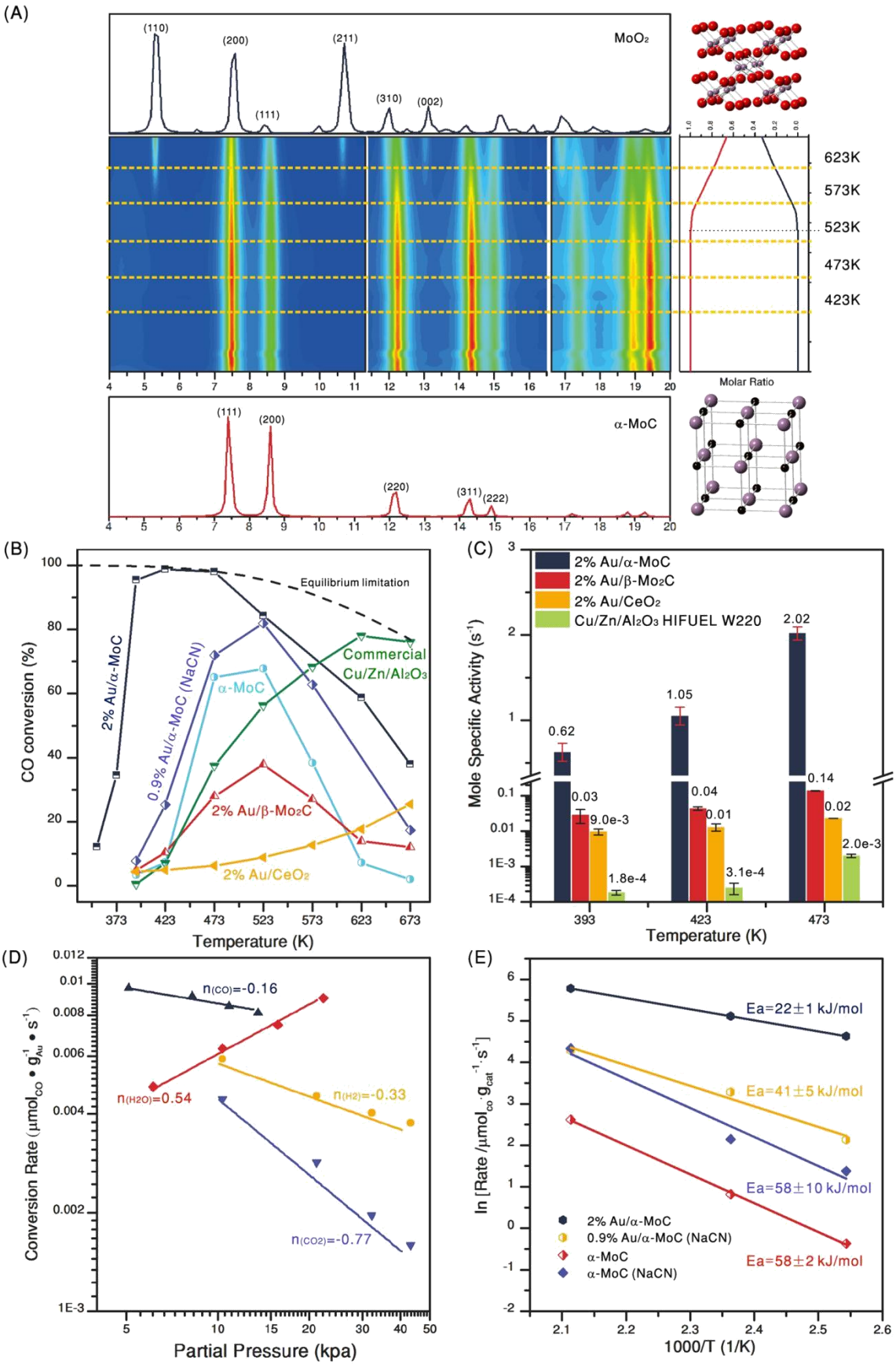
(A)
MoO2
(110)
(200)
(111)
(211)
(310)
(002)
623K
573K
523K
473K
423K
Molar Ratio
α-MoC
(111)
(200)
(220)
(311)
(222)
(B)
Equilibrium limitation
CO conversion (%)
2% Au/α-MoC
0.9% Au/α-MoC (NaCN)
α-MoC
Commercial Cu/Zn/Al2O3
2% Au/β-Mo2C
2% Au/CeO2
Temperature (K)
(C)
2% Au/α-MoC
2% Au/β-Mo2C
2% Au/CeO2
Cu/Zn/Al2O3 HIFUEL W220
Mole Specific Activity (s-1)
0.62
0.03
9.0e-3
1.8e-4
1.05
0.04
0.01
3.1e-4
2.02
0.14
0.02
2.0e-3
Temperature (K)
(D)
n(CO)=-0.16
n(H2O)=0.54
n(H2)=-0.33
n(CO2)=-0.77
Conversion Rate (μmolCO • gAu-1 • s-1)
Partial Pressure (kpa)
(E)
Ea=22±1 kJ/mol
Ea=41±5 kJ/mol
Ea=58±10 kJ/mol
Ea=58±2 kJ/mol
2% Au/α-MoC
0.9% Au/α-MoC (NaCN)
α-MoC
α-MoC (NaCN)
ln [Rate /μmolco·gcat-1·s-1]
1000/T (1/K)

Fig. 1. Catalytic properties and structural characterization of 2% Au/α-MoC catalyst.

(**A**) In-situ XRD (λ=0.3196 Å) of 2% Au/α-MoC catalyst under WGS reaction conditions at various temperatures. (**B**) CO conversion on different catalysts at various temperatures. (Reaction condition*:* 10.5% CO, 21% H_2O, 20% N_2 in Ar; GHSV: 180,000 $hours^{-1}$). (**C**) The activity of different catalysts (unit $mol_{CO}/(mol_{metal}.s)$, (measured at CO conversion below 15% in 11% CO-26% H_2O-26% H_2-7% CO_2-30% N_2). (**D**) Kinetic orders of the reactants and products. (**E**) Apparent activation energy E_{app} of various catalysts in 10.5% CO-21% H_2O-20% N_2-Ar balance.

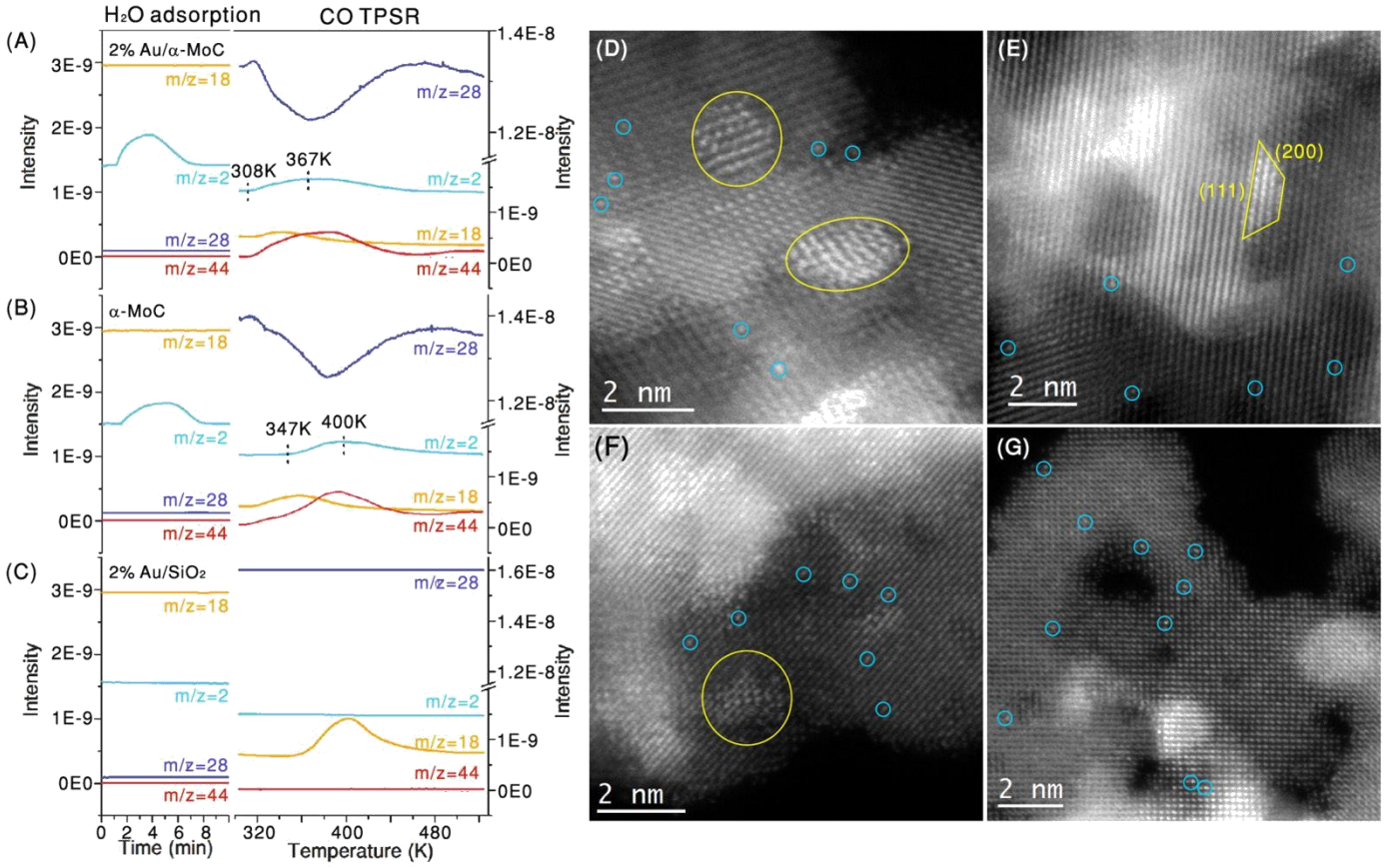

Fig. 2. Mechanism study and electron microscopy characterization. Water adsorption (at 303 K) followed by CO-TPSR on 2% Au/α-MoC (**A**), α-MoC (**B**) and 2% Au/SiO_2 (**C**). Signals of H_2 (m/z=2), H_2O (m/z=18), CO (m/z=28) and CO_2 (m/z=44) were detected. (**D** and **E**) High-resolution HAADF-STEM images of 2% Au/α-MoC fresh catalyst, with single atoms of Au marked in blue circles and Au layered-structures highlighted in yellow. The Au clusters were further identified by elemental analysis (figs. S18 and S19). (**F**) HAADF-STEM image of 2% Au/α-MoC catalyst after reaction in which sample still contains both single-atom Au and Au layered-clusters. (**G**) HAADF-STEM image of the NaCN leached 2% Au/α-MoC catalyst, showing predominantly single atom Au, most of which overlap with Mo sites in the support lattice. Note that the very bright features in this image are caused by overlapping MoC particles, as confirmed by elemental mapping (figs. S18 and S19).

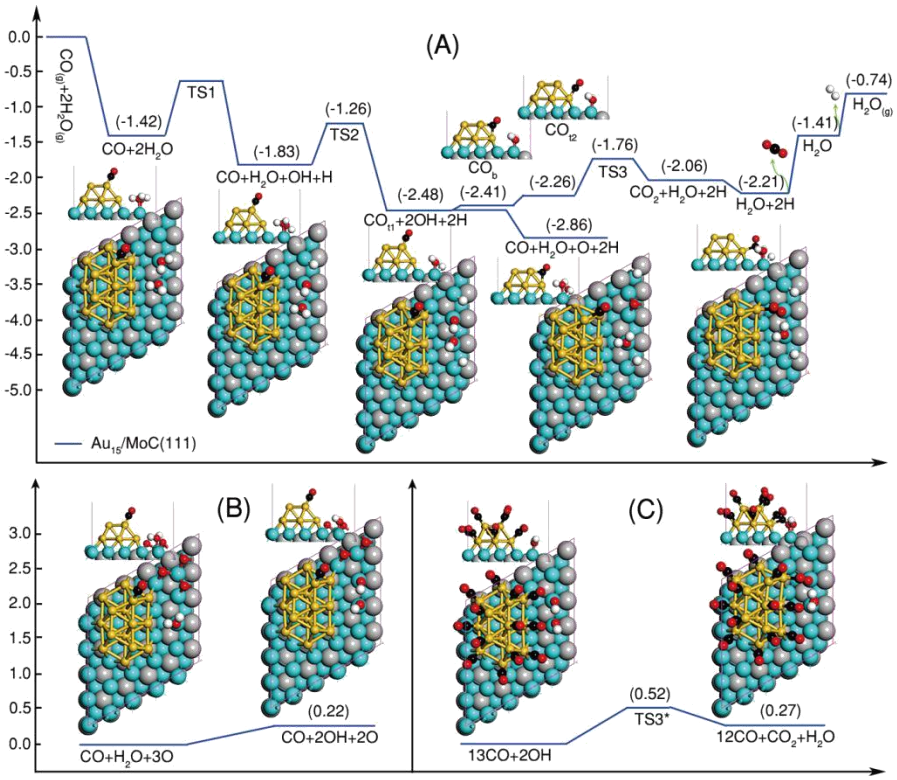

Fig. 3. The reaction paths for the water-gas shift reaction on Au_{15}/α-MoC(111). (**A**) H_2O dissociation and CO reforming at lower coverage, (**B**) O-assisted H_2O dissociation on the boundary oxidized by 3 O atoms and (**C**) CO reforming at high coverage. The energies of gaseous molecules have included the zero-point energy (ZPE) and entropy correction at 423 K. Au, Mo, C, O and H atoms are shown in gold, cyan, gray, red and white, respectively; while in order to make a distinction for the C atom from CO, it is represented by dark gray.